

Monolithic dual-polarization self-mode-locked Nd:YAG 946-nm lasers: controlling beat frequency and observation of temporal chaos

H. P. CHENG, T. L. HUANG, C. Y. LEE, C. L. SUNG, C. Y. CHO, AND Y. F. CHEN*

Department of Electrophysics, National Chiao Tung University, Hsinchu, Taiwan

**yfchen@cc.nctu.edu.tw*

Abstract: The self-mode-locked (SML) operation at 946 nm can be achieved with a monolithic Nd:YAG crystal when the pump power is above the threshold of the multiple-longitudinal-mode generation. The SML output is further found to include two orthogonal polarization components with a beat frequency coming from the birefringence effect in the laser crystal. The beat frequency can be widely adjusted in the range of 5–220 MHz by controlling the cooling temperature. The present experiment also confirms the theoretical prediction that the two-mode operation generally exhibits the chaotic dynamics when the frequency difference is sufficiently close to the relaxation frequency.

© 2016 Optical Society of America

OCIS codes: (140.3480) Lasers, diode-pumped; (140.3530) Lasers, neodymium; (140.4050) Mode-locked lasers; (140.1540) Chaos.

References and Links

1. W. Holzapfel and U. Riss, "Computer-based high resolution transmission ellipsometry," *Appl. Opt.* **26**(1), 145–153 (1987).
2. M. Oka and S. Kubota, "Stable intracavity doubling of orthogonal linearly polarized modes in diode-pumped Nd:YAG lasers," *Opt. Lett.* **13**(10), 805–807 (1988).
3. I. J. Kim, C. M. Kim, H. T. Kim, G. H. Lee, Y. S. Lee, J. Y. Park, D. J. Cho, and C. H. Nam, "Highly efficient high-harmonic generation in an orthogonally polarized two-color laser field," *Phys. Rev. Lett.* **94**(24), 243901 (2005).
4. M. Rosenbluh, V. Shah, S. Knappe, and J. Kitching, "Differentially detected coherent population trapping resonances excited by orthogonally polarized laser fields," *Opt. Express* **14**(15), 6588–6594 (2006).
5. S. L. Zhang, Y. D. Tan, and Y. Li, "Orthogonally polarized dual frequency lasers and applications in self-sensing metrology," *Meas. Sci. Technol.* **21**(5), 054016 (2010).
6. W. Holzapfel and M. Finemann, "High-resolution force sensing by a diode-pumped Nd:YAG laser," *Opt. Lett.* **18**(23), 2062–2064 (1993).
7. S. L. Zhang and W. Holzapfel, *Orthogonal Polarization in Lasers: Physical Phenomena and Engineering Applications* (Wiley, 2013).
8. S. Yang and S. L. Chang, "The frequency split phenomenon in a He-Ne laser with a rotational quartz plate in its cavity," *Opt. Commun.* **68**(1), 55–57 (1988).
9. S. L. Chang, M. Lu, and M. X. Wu, "Laser frequency split by an electro-optical element in its cavity," *Opt. Commun.* **96**(4), 245–248 (1993).
10. A. Owyong and P. Esherick, "Stress-induced tuning of a diode-laser-excited monolithic Nd:YAG laser," *Opt. Lett.* **12**(12), 999–1001 (1987).
11. T. Yoshino and Y. Kobayashi, "Temperature characteristics and stabilization of orthogonal polarization two-frequency Nd³⁺:YAG microchip lasers," *Appl. Opt.* **38**(15), 3266–3270 (1999).
12. A. K. Cousins, "Temperature and thermal stress scaling in finite-length end-pumped laser rods," *IEEE J. Quantum Electron.* **28**(4), 1057–1069 (1992).
13. W. Koechner and D. K. Rice, "Effect of birefringence on the performance of linearly polarized YAG:Nd lasers," *IEEE J. Quantum Electron.* **6**(9), 557–566 (1970).
14. C. W. Xu, D. Y. Tang, H. Y. Zhu, and J. Zhang, "Mode locking of Yb: GdYAG ceramic lasers with an isotropic cavity," *Laser Phys. Lett.* **10**(9), 095702 (2013).
15. M. Spanner, K. M. Davitt, and M. Y. Ivanova, "Stability of angular confinement and rotational acceleration of a diatomic molecule in an optical centrifuge," *J. Chem. Phys.* **115**(18), 8403 (2001).
16. L. Tong, V. D. Miljković, and M. Käll, "Alignment, rotation, and spinning of single plasmonic nanoparticles and nanowires using polarization dependent optical forces," *Nano Lett.* **10**(1), 268–273 (2010).

17. N. Kanda, T. Higuchi, H. Shimizu, K. Konishi, K. Yoshioka, and M. Kuwata-Gonokami, "The vectorial control of magnetization by light," *Nat. Commun.* **2**, 362 (2011).
18. G. D. VanWiggeren and R. Roy, "Communication with dynamically fluctuating states of light polarization," *Phys. Rev. Lett.* **88**(9), 097903 (2002).
19. C. L. Sung, H. P. Cheng, C. Y. Lee, C. Y. Cho, H. C. Liang, and Y. F. Chen, "Generation of orthogonally polarized self-mode-locked Nd:YAG lasers with tunable beat frequencies from the thermally induced birefringence," *Opt. Lett.* **41**(8), 1781–1784 (2016).
20. G. Q. Xie, D. Y. Tang, L. M. Zhao, L. J. Qian, and K. Ueda, "High-power self-mode-locked Yb:Y₂O₃ ceramic laser," *Opt. Lett.* **32**(18), 2741–2743 (2007).
21. A. Lagatsky, C. Brown, and W. Sibbett, "Highly efficient and low threshold diode-pumped Kerr-lens mode-locked Yb:KYW laser," *Opt. Express* **12**(17), 3928–3933 (2004).
22. H. C. Liang, H. L. Chang, W. C. Huang, K. W. Su, Y. F. Chen, and Y. T. Chen, "Self-mode-locked Nd:GdVO₄ laser with multi-GHz oscillations: manifestation of third-order nonlinearity," *Appl. Phys. B* **97**(2), 451–455 (2009).
23. H. C. Liang, Y. J. Huang, W. C. Huang, K. W. Su, and Y. F. Chen, "High-power, diode-end-pumped, multigigahertz self-mode-locked Nd:YVO₄ laser at 1342 nm," *Opt. Lett.* **35**(1), 4–6 (2010).
24. F. Krausz, T. Brabec, and C. Spielmann, "Self-starting passive mode locking," *Opt. Lett.* **16**(4), 235–237 (1991).
25. W. Z. Zhuang, M. T. Chang, H. C. Liang, and Y. F. Chen, "High-power high-repetition-rate subpicosecond monolithic Yb:KGW laser with self-mode locking," *Opt. Lett.* **38**(14), 2596–2599 (2013).
26. C. Y. Lee, C. C. Chang, H. C. Liang, and Y. F. Chen, "Frequency comb expansion in a monolithic self-mode-locked laser concurrent with stimulated Raman scattering," *Laser Photonics Rev.* **8**(5), 750–755 (2014).
27. Y. F. Chen, M. T. Chang, W. Z. Zhuang, K. W. Su, K. F. Huang, and H. C. Liang, "Generation of sub-terahertz repetition rates from a monolithic self-mode-locked laser coupled with an external Fabry-Perot cavity," *Laser Photonics Rev.* **9**(1), 91–97 (2015).
28. M. T. Chang, H. C. Liang, K. W. Su, and Y. F. Chen, "Dual-comb self-mode-locked monolithic Yb:KGW laser with orthogonal polarizations," *Opt. Express* **23**(8), 10111–10116 (2015).
29. D. W. Chen, C. L. Fincher, T. S. Rose, F. L. Vernon, and R. A. Fields, "Diode-pumped 1-W continuous-wave Er:YAG 3- μ m laser," *Opt. Lett.* **24**(6), 385–387 (1999).
30. Y. J. Chen, Y. F. Lin, J. H. Huang, X. H. Gong, Z. D. Luo, and Y. D. Huang, "Diode-pumped monolithic Er³⁺:Yb³⁺:YAl₃(BO₃)₄ micro-laser at 1.6 μ m," *Opt. Commun.* **285**(5), 751–754 (2012).
31. T. R. Schibli, T. Kremp, U. Morgner, F. X. Kärtner, R. Butendeich, J. Schwarz, H. Schweizer, F. Scholz, J. Hetzler, and M. Wegener, "Continuous-wave operation and Q-switched mode locking of Cr⁴⁺:YAG microchip lasers," *Opt. Lett.* **26**(12), 941–943 (2001).
32. S. Zhou, K. K. Lee, Y. C. Chen, and S. Li, "Monolithic self-Q-switched Cr,Nd:YAG laser," *Opt. Lett.* **18**(7), 511–512 (1993).
33. R. S. Conroy, T. Lake, G. J. Friel, A. J. Kemp, and B. D. Sinclair, "Self-Q-switched Nd:YVO₄ microchip lasers," *Opt. Lett.* **23**(6), 457–459 (1998).
34. J. Dong, K. Ueda, A. Shirakawa, H. Yagi, T. Yanagitani, and A. A. Kaminskii, "Composite Yb:YAG/Cr⁴⁺:YAG ceramics picosecond microchip lasers," *Opt. Express* **15**(22), 14516–14523 (2007).
35. N. Pavel, M. Tsunekane, and T. Taira, "Composite, all-ceramics, high-peak power Nd:YAG/Cr⁴⁺:YAG monolithic micro-laser with multiple-beam output for engine ignition," *Opt. Express* **19**(10), 9378–9384 (2011).
36. N. V. Kravtsov and E. G. E. Lariontsev, "Self-modulation oscillations and relaxation processes in solid-state ring lasers," *Quantum Electron.* **24**(10), 841–856 (1994).
37. I. I. Zolotovikh, N. V. Kravtsov, E. G. E. Lariontsev, A. A. Makarov, and V. V. Firsov, "New mechanisms of the appearance of dynamic chaos in a ring solid-state laser," *Quantum Electron.* **25**(3), 197–199 (1995).
38. Y. F. Chen and Y. P. Lan, "Dynamics of helical-wave emission in a fiber-coupled diode end-pumped solid-state laser," *Appl. Phys. B* **73**(1), 11–14 (2001).
39. T. Heil, I. Fischer, W. Elsässer, and A. Gavrielides, "Dynamics of semiconductor lasers subject to delayed optical feedback: the short cavity regime," *Phys. Rev. Lett.* **87**(24), 243901 (2001).
40. J. Ding, Q. Feng, L. Zhang, and S. Zhang, "Laser frequency splitting method for high-resolution determination of relative stress-optic coefficient and internal stresses in Nd:YAG crystals," *Appl. Opt.* **47**(30), 5631–5636 (2008).
41. A. Kuske and G. Robertson, *Photoelastic Stress Analysis* (Wiley, 1974), pp. 88 and 108–110.
42. W. Koehnner, *Solid-State Laser Engineering* (Springer-Verlag, 2006), Chap. 2.

1. Introduction

Orthogonally polarized dual-frequency (OPDF) lasers are attractive for many applications, such as optical navigation, military purpose, medical surgery, material processing and high-resolution measurement [1–7]. One typical method for generating the OPDF laser is to insert a birefringent element into the laser cavity to split the laser frequency between two orthogonal states [7–9]. Alternatively, the OPDF laser can be generated by introducing the induced birefringence into an isotropic gain medium, such as Nd:YAG crystal. The induced

birefringence [10–14] that may come from the residual stress, external force or thermal stress can lead to a frequency difference between two orthogonally polarized modes.

The realization of the mode-locked operation in the OPDF lasers is greatly useful for numerous practical applications, such as in angular trapping and rotational acceleration of a diatomic molecule, in vectorial control of magnetization, and in optical communication [14–18]. Recently, the self-mode-locked (SML) operation in an OPDF YAG 1064-nm laser has been successfully demonstrated by using a simple linear cavity without any additional saturable absorber [14,19]. The fundamental mechanisms for achieving the SML operation are the nonlinearity of the gain medium itself and the soft aperture formed by the end-pumping scheme [20–23]. Both theoretical and experimental results confirm that an increase in the longitudinal mode spacing is effectively beneficial to the SML operation [24–26]. Consequently, the monolithic resonator with large mode spacing is particularly suitable for the SML operation [25–28]. In the early stages, monolithic or bonded cavities were often used in developing the continuous-wave [29–31] and passively Q-switched lasers [32–35] due to the advantage of mechanical stability, compact, and alignment-free manufacturing.

Lasers with wavelength in the range of 0.9 μm are practically useful in the remote sensing and the generation of blue lasers by using second harmonic generation for underwater communications and display technologies. In this work, we explore the laser performance of a diode-end-pumped Nd:YAG crystal with the coating to form a monolithic 946-nm cavity. Experimental results reveal that the SML operation can be naturally achieved as long as the pump power is high enough for the multiple-longitudinal-mode generation. At an incident pump power of 2.9 W, the monolithic laser can efficiently generate a total output power of 460 mW with a pulse repetition rate of 12.6 GHz that corresponds to the crystal length of 6.5 mm very well. Furthermore, the polarization-resolved measurement shows that the SML output consists of two orthogonal polarization components along the vertical and horizontal directions. It is also found that the central frequency difference between two orthogonally polarized mode-locked states leads to a beating modulation in the temporal characteristics. It is experimentally confirmed that the birefringence effect of the laser crystal mainly comes from the temperature difference between side walls and bottom wall of the crystal holder. As a result, the beat frequency can be directly adjusted by controlling the temperature of the bottom wall of the crystal holder. The beat frequency is down to the minimum when the controlling temperature is close to the environment temperature. The adjustable range of the beat frequency is approximately 220 MHz for the temperature decreasing from 27 $^{\circ}\text{C}$ to 10 $^{\circ}\text{C}$. It is intriguingly found that the laser output usually displays the chaotic temporal dynamics when the beat frequency is in the region of the minimum and close to the relaxation oscillation frequency. The appearance of dynamic chaos was well consistent with the laser theory for the interaction of two-mode class-B laser sources with the relaxation oscillation [36–38]. This finding indicates that the present system can pave a way to explore the laser dynamics arising from the interaction between the relaxation oscillation and the beat modulation of two orthogonal polarizations in class-B lasers.

2. Experimental setup

The experimental setup for the monolithic Nd:YAG laser is shown in Fig. 1(a). The gain medium was a 1.1-at. % Nd:YAG crystal with a length of 6.5 mm and a transverse aperture of $3 \times 3 \text{ mm}^2$. End surfaces of the gain medium had the coatings to form a monolithic cavity at 946 nm. The front surface of the Nd:YAG crystal had the high-reflection coating (HR, $R > 99.9\%$) at 946 nm for resonance, the high-transmission coating (HT, $T > 95\%$) at 808 nm for transmitting the pump light, the high-transmission coating ($T > 90\%$) at 1064 nm and 1320 nm for suppression. The output surface had the partial-reflection coating (PR, $R = 97\%$) at 946 nm for output emission and the high-transmission coating ($T > 90\%$) at 1064 nm and 1320 nm for suppression. The gain medium was wrapped with indium foil and mounted in a copper holder, as shown in Fig. 1(b) for the end view. The bottom wall of the copper holder

was water-cooled with a precise temperature controller. Note that the temperature of the side walls of the copper holder was slightly different from the bottom wall due to the thermal resistances contributed by the heat conduction to the bottom wall and the heat convection to the surrounding.

The pump source was a 3-W 808-nm fiber-coupled laser diode with a 200- μm fiber core diameter and a numerical aperture of 0.16. The pump light was focused into the gain medium by using a lens with the focal length of 50 mm for collimation and a lens with the focal length of 25 mm for focusing. The radius of the pump beam in the Nd:YAG crystal was approximately 50 μm . The mode-locked pulse train was detected by a high-speed InGaAs photodetector (Electro-Optics Technology Inc. ET-3500 with rising time 35 ps) and the output signals were connected to a digital oscilloscope (Teledyne LeCroy WaveMaster 820Zi-A) with 20 GHz electrical bandwidth and a sampling interval of 25 ps. At the same time, the output signal of the photodetector was also delivered to a RF spectrum analyzer (Agilent, 8563EC) with bandwidth of 9 kHz to 26.5 GHz. A Fourier optical spectrum analyzer (Advantest Q8347), which was formed with a Michelson interferometer, was applied to monitor the spectral information with the resolution of 0.003 nm.

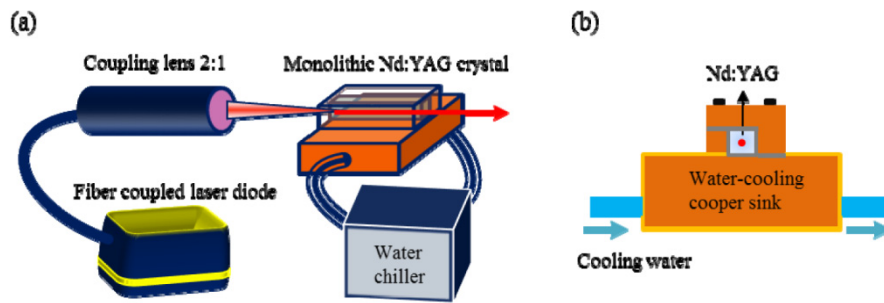


Fig. 1. (a) Experimental setup for the monolithic Nd:YAG laser at 946 nm; (b) end view of the crystal holder with the water cooling.

3. Dual-polarization self-mode-locked operation

To begin with, the water temperature for cooling the holder was set at 15 °C to observe the overall performance. Figure 2 demonstrates the temporal trace and the RF spectrum at an incident pump power of 1.04 times the lasing threshold. The relaxation frequency f_r and its harmonics can be observed in the RF spectrum. It can be seen that the output intensities consist of a low-frequency envelop that forms the quasi-periodic pulse packages [39]. Figure 3(a) shows the experimental result for the output power versus the incident pump power. The average output power reached 460 mW at an incident power of 2.9 W, corresponding to a slope efficiency of approximately 21.5%. The optical spectrum of the lasing output at the maximum pump power of 2.9 W is depicted in Fig. 3(b). The structure of the multiple longitudinal modes can be clearly seen because the mode spacing is large enough for resolving. It was experimentally confirmed that the number of the longitudinal lasing modes was approximately 6–8 for the pump power greater than 1.1 times the lasing threshold.

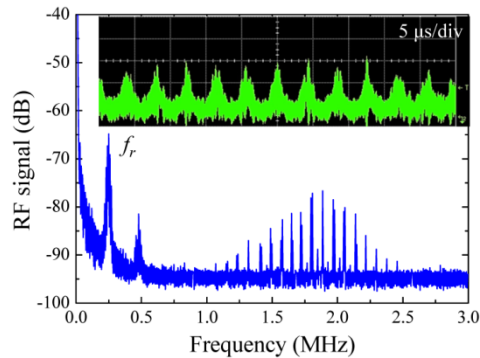


Fig. 2. RF power spectrum and the temporal trace at a pump power of 1.04 times the lasing threshold.

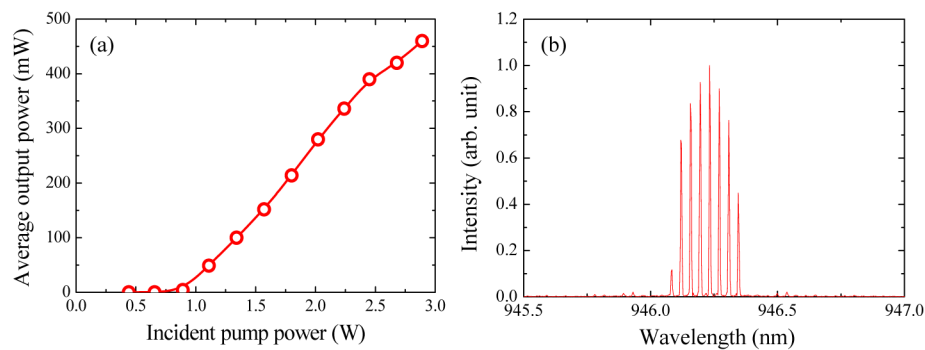


Fig. 3. (a) Experimental result for the output power versus the incident pump; (b) optical spectrum of the lasing output at the maximum pump power.

The oscilloscope traces of the total output intensity revealed that the lasing emission naturally stepped into the SML operation when the pump power is sufficiently high for the multiple-longitudinal-mode oscillation. Typical oscilloscope traces of the mode-locked pulse trains at a pump power of 2.5 W are illustrated in Figs. 4(a) and 4(b) with the time span of 50 ns and 2 ns, respectively. Figure 4(a) illustrates the stability of the SML laser, and the fluctuation can be seen to be better than 2%. On the other hand, the pulse period in Fig. 4(b) is approximately 79.3 ps, which agrees very well with the round trip time of the monolithic cavity. Figure 4(c) depicts the autocorrelation trace of the mode-locked pulse train with the delay time of 60 ps. The FWHM of the autocorrelation trace is measured to be about 10.7 ps. With the Gaussian-shaped temporal profile for analysis, the pulse width of the autocorrelation trace was found to be approximately 7.6 ps.

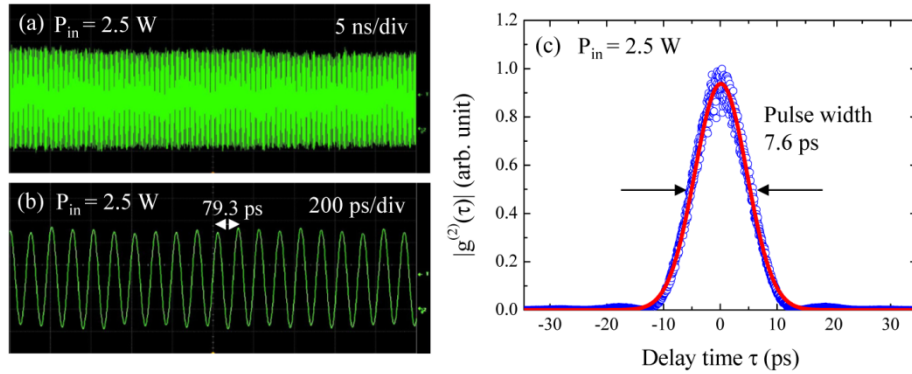


Fig. 4. Oscilloscope traces with the time span of: (a) 50 ns and (b) 2 ns for the mode-locked operation; (c) autocorrelation trace of the output pulses.

Next, we measured the polarization-resolved temporal traces to explore the polarization state of the output emission. We found that the lasing output was composed of two orthogonally polarized eigenstates with different central frequencies. The two orthogonally polarized eigenstates were found to be along the horizontal (x) and vertical (y) directions with respect to the bottom wall of the holder. Figures 5(a)-5(d) show the oscilloscope traces for the polarization-resolved output intensities I_θ at $\theta = 0^\circ$, $\theta = 90^\circ$, $\theta = 45^\circ$ and $\theta = 135^\circ$ at an incident pump power of 2.5 W, respectively, where θ is the analyzer angle with respect to the x axis. The pulse trains for two orthogonal eigenstates at $\theta = 0^\circ$ and $\theta = 90^\circ$ can be seen to be almost identical to the feature of the total output intensity. On the other hand, the polarization-resolved output intensities at $\theta = 45^\circ$ and $\theta = 135^\circ$ displayed a phenomenon of intensity modulation with a beat frequency of 167 MHz, as seen in Figs. 5(c) and 5(d). It was further verified that the beating modulation trace were completely antiphase between $\theta = 45^\circ$ and $\theta = 135^\circ$. The appearance of the beat frequency indicates the existence of the birefringence effect in the laser crystal.

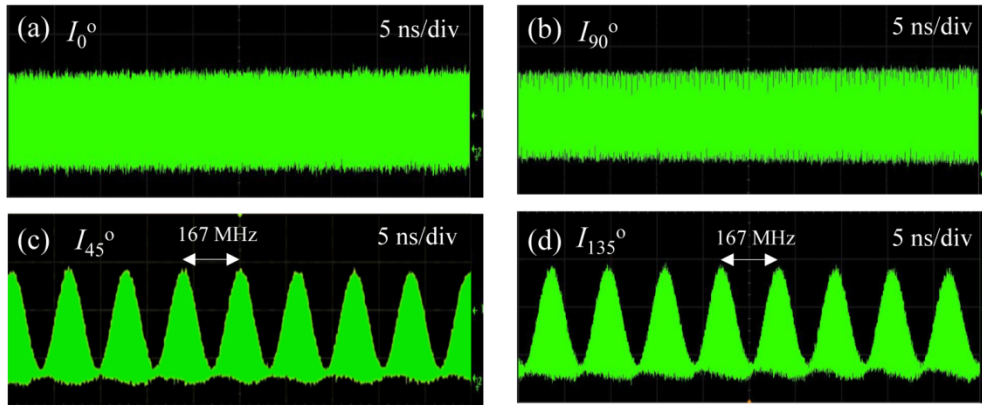


Fig. 5. Pulse trains of the polarization-resolved output intensities $I_\theta(t)$ at a pump power of 2.5 W: (a) $\theta = 0^\circ$; (b) $\theta = 90^\circ$; (c) $\theta = 45^\circ$; and (d) $\theta = 135^\circ$.

4. Controlling beat frequency and emergence of temporal chaos

We made further experimental and theoretical studies to verify that the origin of the birefringence effect in the laser crystal mainly came from the temperature difference ΔT between the side walls and the bottom wall of the copper holder. Figure 6(a) shows the total output power versus the water cooling temperature T_c at a pump power 2.0 W. The total

output power obviously decreased from 333 mW to 230 mW with increasing the temperature from 10 °C to 35 °C. The output power reduction was mainly due to the increased reabsorption loss with increasing temperature. Not only the output power but also the beat frequency changed with the water cooling temperature, as shown in Fig. 6(b). It can be seen that the beat frequency is up to 222 MHz at $T_c = 10$ °C and down to the minimum for T_c close to the surrounding temperature $T_s = 27$ °C. The minimal value of the observable beat frequency was approximately 5 MHz. Figures 6(c) and 6(d) show the polarization-resolved output intensities I_θ with $\theta = 45^\circ$ at $T_c = 10$ °C and 27 °C, respectively. This result implies that the birefringence effect in the laser crystal depends on the water cooling temperature. When the water temperature was higher than the surrounding temperature, the beat frequency started to rise to 56 MHz at $T_c = 35$ °C, indicating the increasing of the birefringence. To be brief, the magnitude of the birefringence can be effectively varied by controlling the temperature difference between the water and the surrounding.

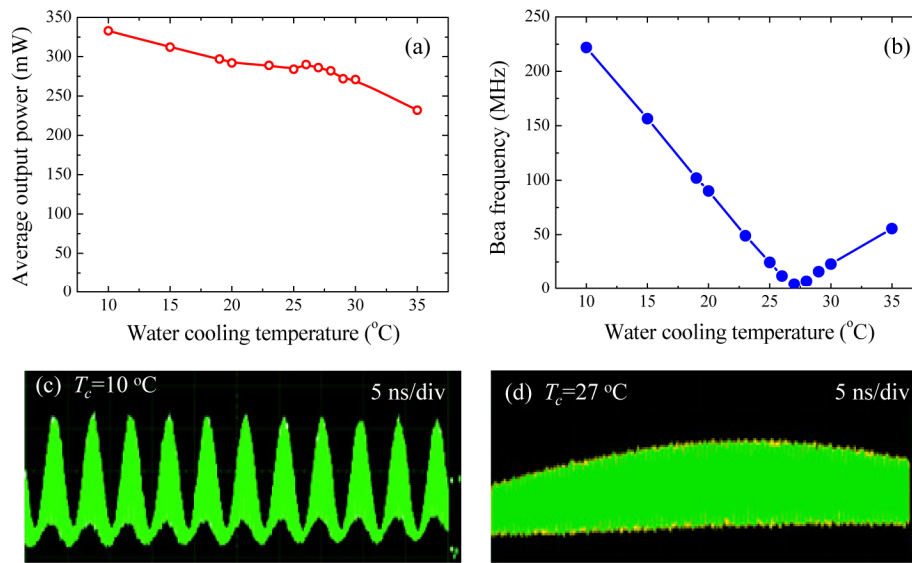


Fig. 6. (a) Total output power versus the water cooling temperature T_c at a pump power 2.0 W; (b) beat frequency versus with the water cooling temperature; (c) polarization-resolved output intensity $I_{45^\circ}(t)$ at $T_c = 10$ °C; (d) polarization-resolved output intensity $I_{45^\circ}(t)$ at $T_c = 27$ °C.

Considering the birefringence effect in the monolithic cavity, the frequency difference between the two orthogonal polarization states is given by equation:

$$\Delta f = f \frac{\Delta L}{nL_{cry}}, \quad (1)$$

where f is laser frequency, n is the refractive index, L_{cry} is the geometric length of the laser crystal, and ΔL is the difference of the optical cavity length between two polarization states. Using the stress-optic law of two-dimensional photoelasticity, the optical path difference of the photoelastic material is given by [40,41]:

$$\Delta L = C L_{cry} \Delta \sigma, \quad (2)$$

where C is the relative stress-optic coefficient and $\Delta \sigma$ is the principal stress difference. The principle stress difference $\Delta \sigma$ is related to the temperature difference ΔT between the side and bottom surfaces of the Nd:YAG crystal, which approximately corresponds to the temperature difference between the side walls and the bottom wall of the copper holder, respectively. The

bottom wall of the copper holder is nearly determined by the water cooling temperature T_c . Subject to the influence of the surrounding temperature, the average temperature at the side walls of the copper holder can be approximated as $T_a = T_c + \mu(T_s - T_c)$, where μ is a positive coefficient and $\mu \ll 1$. The coefficient μ was experimentally measured to be approximately 0.025 for $T_c \leq T_s$. To be brief, $\Delta T = T_a - T_c = \mu(T_s - T_c)$. For the stress due to the thermal expansion of the Nd:YAG crystal, the principal stress difference $\Delta\sigma$ can be given by:

$$\Delta\sigma = E\alpha_T \Delta T, \quad (3)$$

where E is the Young's Modulus and α_T is the thermal expansion coefficient of the laser crystal. Substituting Eqs. (2) and (3) into Eq. (1), the frequency difference Δf can be expressed as:

$$\frac{\Delta f}{T_s - T_c} = f \frac{C}{n} E \alpha_T \mu. \quad (4)$$

Using the parameter values of $f = 3.17 \times 10^{14}$ Hz, $C = 1.25 \times 10^{-12}$ m²/N [41], $n = 1.82$, $E = 310$ GPa [42], $\alpha_T = 7.5 \times 10^{-6}$ [42], and $\mu = 0.025$, the variation of the beat frequency with the temperature difference can be calculated to be $\Delta f / (T_s - T_c) = 12.6$ MHz/°C. This result is fairly consistent with the experimental result of 12.8 MHz/°C shown in Fig. 6(b) for the region of $T_c < T_s$.

Finally, it is worthwhile to mention the observation of the temporal dynamics near the condition of $T_c \approx T_s$. Figure 7(a) shows the RF power spectrum and the temporal trace for the polarization-resolved output intensity at $T_c \rightarrow T_s$ from the lower temperature at a pump power of 2.0 W. It can be seen that the beat frequency is approximately 5.5 MHz and becomes broader in the RF spectrum. Furthermore, the frequency f_r and harmonics of the relaxation oscillation can also be observed in the RF spectrum. Under this circumstance, the temporal trace of the output intensity at a pump power of 2.0 W, as shown in Fig. 7(b), is usually inclined to display the chaotic oscillation through increasing a tiny temperature. The polarization-resolve output intensity $I_{135^\circ}(t)$ also indicates the same phenomenon in the RF spectrum and temporal trace, as shown in Figs. 7(c) and 7(d), respectively. The both modes seem to display outphase chaos between $\theta = 45^\circ$ and $\theta = 135^\circ$. It has been theoretically verified [36–38] that the two-mode operation in the class-B laser systems generally exhibits the chaotic dynamics when the frequency difference is rather close to the relaxation frequency, i.e., $\Delta f \rightarrow f_r$. The present observation agrees very well with the theoretical prediction.

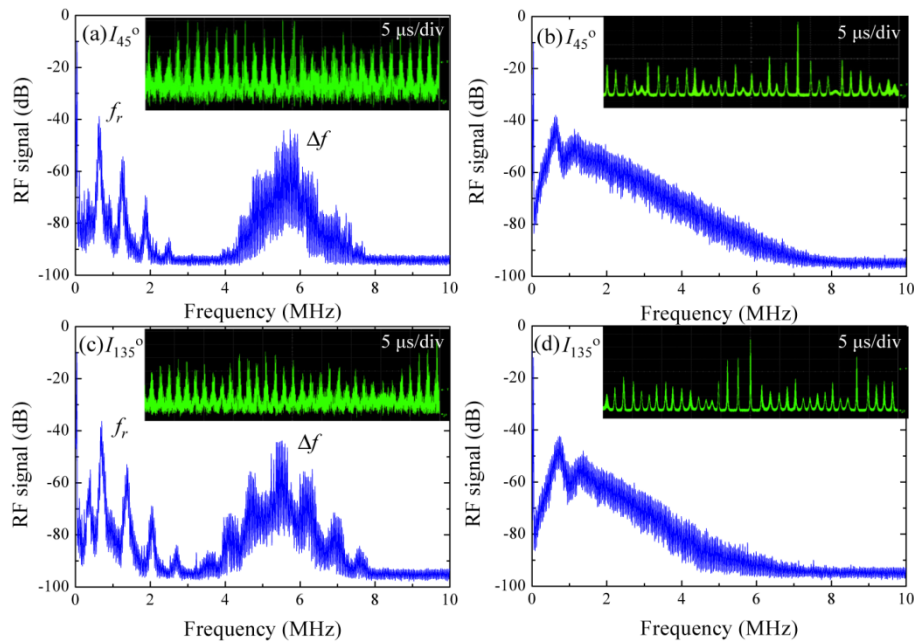


Fig. 7. RF power spectrum and the temporal trace at a pump power of 2.0 W for the polarization-resolved output intensity $I_{45^\circ}(t)$ (a) at $T_c \rightarrow T_s$ from the lower temperature and (b) chaotic dynamics with increasing a tiny temperature; as well as for the polarization-resolved output intensity $I_{135^\circ}(t)$ (c) at $T_c \rightarrow T_s$ from the lower temperature and (d) chaotic dynamics with increasing a tiny temperature.

5. Conclusion

In conclusion, we have experimentally investigated the laser performance of an diode-end-pumped monolithic Nd:YAG laser at 946 nm. It was found that the SML operation with a pulse repetition rate of 12.6 GHz could be naturally achieved when the pump power was greater than the threshold of the multiple-longitudinal-mode generation. The output power can be up to 460 mW at an incident pump power of 2.9 W. It was also found that the SML output was composed of two orthogonal polarization components with a central frequency difference to lead to a beating modulation in the temporal characteristics. We further confirmed that the origin of the beat frequency was the birefringence effect in the laser crystal mainly induced by the temperature difference between the side and bottom surfaces of the Nd:YAG crystal. By controlling the water temperature between 10–27 °C, the beat frequency can be widely adjusted in the range of 5–220 MHz. More interestingly, the present experiment confirms the theoretical prediction that the two-mode operation in the class-B laser systems generally exhibits the chaotic dynamics when the frequency difference is rather close to the relaxation frequency.

Acknowledgments

The authors thank the Ministry of Science and Technology of Taiwan for the financial support of this research under Contract No. MOST 105-2628-M-009-004.